Supplementary Information

1. Experimental sectional

1.1 Materials Preparation

The LiTFSI (99.9 %, Sigma-Aldrich) WIS solution was prepared in an Ar-filled glove box. For concentrations higher than 30 m, the samples needed to be heated for several minutes at slightly elevated temperature to form a homogeneous solution.

The electrode for galvanostatic polarization measurement is prepared by mixing $LiFePO_4$ (Sigma-Aldrich), Polyvinylidenfluorid (PVDF, Sigmar-Aldrich) and carbon black with N-Methyl-2-pyrrolidon (NMP). The ratio of materials was 8:1:1. As prepared slurry is casted on the Cu foils and then heated in the oven overnight.

1.2 Electrochemical Characterization

Ionic Conductivity

The ionic conductivity is measured in the self-made T-Cell, with a Pt electrode on both sides. The cell is sealed and placed into the oil bath to maintain the defined temperature (Lauda BC3). The temperature range for the measurement was ranging from -10 to 100 ℃ or 120 ℃. The time interval between each temperature change was set to 30 minutes. The alternating current (AC) measurement is performed by HP 4192A impedance analyzer. Before the measurement of R_{WIS}, the calibration is performed by measuring the resistance of 1 M KCl standard solution, R_{KCl}. The resistances are considered to be the intersections of (in this case extension of) the EIS curve with the X-axis.

The AC conductivity σ_{WIS} is calculated by the following equation:

$$\sigma_{KCl} \cdot R_{KCl} = \sigma_{WIS} \cdot R_{WIS}$$

Transference number $t_{Li,pol}$

For transference number measurements (t_{Li}), different approaches are needed to measure the WIS with different salt concentration. For 21 m aqueous solution:

$LiFePO_4$ electrode materials were firstly prepared, then Li^+ was extracted (to roughly $Li_{0.5}FePO_4$) via full cell charge/discharge. After that, the symmetric Swagelok cell was prepared in the glovebox. Next, AC measurement is performed to determine the current value needed for direct current (DC) measurement. Impedance spectroscopy was measured in a frequency range from 10 MHz to 1 mHz using a Solartron 1260 frequency analyzer. The constant current applied by DC measurement is calculated from $(0.01/R_{SEI,0})$ A where $R_{Sei,0}$ corresponds to the fitted curve around 1 Hz or the first semicircle in the Nyquist diagram. After the potential saturated to a constant value $U_{infinite}$, another AC measurement in the same frequency range is performed to obtain $R_{sei,infinite}$. The $t_{Li,pol}$ is calculated by

$$t_{Li,\,pol} = \frac{I \cdot R_{sei,infinite}}{U_{infinite}}.$$

For 30-55.5 m, the former way of measurement is not possible due to the solidification of the electrolyte in the large time scale and the contact issues when a porous electrode (LFP) was used. The electrode was thus exchange into lithium metal. The calculation and measurement procedure remains the same.

The calculation of σ_+, σ_- and their relationship with the transference number.

The σ_+, σ_- and s are namely the conductivities of the cation, anion and ion pairs. σ_{pol}, σ_{AC} correspond to the steady state DC conductivity and AC conductivity of the electrolyte.

The σ_{pol} is calculated by:

$$\sigma_{pol} = \sigma_{Li^+} + 2\sigma_{Li_2X^+} - \sigma_{LiX_2^-} + \left(\frac{1}{\sigma_{X^-} + 2\sigma_{LiX_2^-} - \sigma_{Li_2X^+}} + \frac{1}{s + 2\sigma_{LiX_2^-} + 2\sigma_{Li_2X^+}}\right)^{-1}$$

and σ_{AC} is calculated by:

$$\sigma_{AC} = \sigma_{Li^+} + \sigma_{X^-} + \sigma_{LiX_2^-} + \sigma_{Li_2X^+}.$$

When s is dominating the ion transport, $\sigma_{LiX_2^-} = \sigma_{Li_2X^+} = 0$, the σ_{pol} and σ_{AC} will

be:

$$\sigma_{pol} = \sigma_{Li^+} + \left(\frac{1}{\sigma_{X^-}} + \frac{1}{s}\right)^{-1}$$

$$\sigma_{AC} = \sigma_{Li^+} + \sigma_{X^-}.$$

When Li_2X^+ is dominating the ion transport, s and $\sigma_{LiX_2^-}$ are 0, then the σ_{pol} and σ_{AC} will be:

$$\sigma_{pol} = \sigma_{Li^+} + 2\sigma_{Li_2X^+} + \left(\frac{1}{\sigma_{X^-} - \sigma_{Li_2X^+}} + \frac{1}{2\sigma_{Li_2X^+}}\right)^{-1}$$

$$\sigma_{AC} = \sigma_{Li^+} + \sigma_{X^-} + \sigma_{Li_2X^+}.$$

When LiX_2^- is dominating the ion transport, s and $\sigma_{Li_2X^+}$ are 0, then the σ_{pol} and σ_{AC} will be:

$$\sigma_{pol} = \sigma_{Li^+} - \sigma_{LiX_2^-} + \left(\frac{1}{\sigma_{X^-} + 2\sigma_{LiX_2^-}} + \frac{1}{2\sigma_{LiX_2^-}}\right)^{-1}$$

$$\sigma_{AC} = \sigma_{Li^+} + \sigma_{X^-} + \sigma_{Li_2X^+}.$$

Fig. S7 shows the transference number $t_{pol} \equiv \frac{\sigma_{pol}}{\sigma AC}$ calculated for different cases under the simplified assumption that $\sigma_{Li^+} = \sigma_{X^-}$. In contrast to neutral associates, charged ones – in particular negatively charged ones – can explain the experimentally observed discrepancy between transference numbers derived from polarization experiments and those derived from PFG-NMR.

1.3 Physico-chemical properties

Raman Spectra

The sample for Raman measurement was sealed in a quartz container and measured on a Renishaw inVia Reflex device at the University of Science and Technology of China. The used wavelength was 532 nm. The data was fitted by Magicplot software.

Magic angle spinning (MAS)-NMR

^{6}Li MAS NMR measurements were performed on a Bruker Avance – III 400 MHz spectrometer (magnetic field of 9.4 T, ^{6}Li Larmor frequency of 58.86 MHz) using a Bruker 4 mm BL4 WVT probe at spinning speeds between 3 and 4 kHz. The spectra were collected using a simple Bloch decay (π/10-pulse-acquire-delay) with π/2-pulse for ^{6}Li being 6.4 μs. ^{6}Li spectra are referenced to 2 M aqueous solution of LiCl (δ_{iso} = 0.0 ppm).[4] Between 64 and 128 scans with relaxation delays between 30 and 50 s were accumulated for a good signal-to-noise ratio. Such a short excitation pulse and long relaxation delays ensured a complete relaxation of the nuclear magnetization and quantitative ratio of signals in the spectra. During the MAS experiments the temperature of the samples was controlled using a Bruker BVT3000 temperature controller and was calibrated using the ^{207}Pb signal in $Pb(NO_3)_2$.[5] Analytical simulations and integration of experimental spectra were carried out with the DMFit and Bruker TopSpin 3.6 Lineshape Analysis Tool simulation packages.[6,7]

Pulsed field gradient NMR (PFG-NMR)

^{7}Li and ^{19}F NMR spectra and Pulse Field Gradient (PFG) NMR measurements were performed on a Bruker Avance-III 400 MHz instrument (magnetic field of 9.4 T, and the Larmor frequencies of ^{7}Li and ^{19}F are 155.56 MHz and 376.498 MHz, respectively), equipped with a diff30 single gradient diffusion probe. The probe allows for pulse field gradients g of up to 20 T/m and variable temperature measurements up to +120 ^{o}C. The diffusion measurements were accomplished using a Stimulated Echo pulse sequence with bipolar field gradients. [8] The echo attenuation curves $S(g,\delta,\Delta)$ were processed using the Stejscal-Tanner equation, $S(g,\delta,\Delta)=\exp(-\gamma^2\delta^2g^2D(\Delta-\delta/3))$, where γ is the gyromagnetic ratio of the studied nucleus ($\gamma(^{7}Li) = 10.398 \times 10^{7}$ rad s^{-1} T^{-1}, ($\gamma(^{19}F)$ = 25.162 rad s^{-1} T^{-1}), g is the strength

of the pulse field gradient of duration δ, D is the effective diffusion coefficient, and Δ is the time interval between the field gradients that defines the diffusion time scale. [9] We note, that the use of bipolar gradients provided an effective compensation of convection in molten samples, that may contribute to the measurement above 313 K. As the experiment's diffusion times are on the millisecond scale and the respective species exchange faster, the measured diffusion coefficients are weighted averages of the diffusion coefficients of all species containing the specific nucleus.[10]

Using the Stejscal-Tanner equation above, the experimental diffusion coefficients D have been obtained by fitting experimental echo intensities at incrementing gradient strength. [9,11] All diffusion coefficients were measured for a constant Δ = 100 ms (no dependence on the diffusion time down to Δ = 20 ms has been noticed), and for an effective gradient duration δ = 1 ms. Re-magnetization times were chosen to be 4 to 5 times higher than the spin-lattice relaxation time, T_1.

DSC

The DSC was measured by Netzsch DSC 214, the temperature ramp is 5 K per minute from -60 ℃ to 150 ℃.

Viscosity

Viscosity was measured by Malvern Kinexus device in the form of sheer viscosity as the solidification is easy to occur when the sample attaches on the plate. The temperature for measuring the data necessary for the Walden plot is 80 ℃.

XRD

Samples were sealed in a quartz capillary (diameter 1.0 mm). The powder X-ray diffraction (PXRD) patterns were collected on a STOE Stadi-P diffractometer with Cu-$K_{\alpha 1}$ radiation (λ = 1.540596 Å), equipped with a Ge(111) Johann monochromator, and an array of three DECTRIS Mythen 1K detectors in Debye-

Scherrer geometry over an angular range of 0–55.050° 2θ. The capillary was spun during the measurement to improve the crystallite orientation sampling statistics. Heating of the sample was performed using an Oxford Cryostream over intervals between -20 to 120 ℃ in steps of either 5, 10, or 20 ℃ depending on temperature range. Rietveld and Pawley refinements to determine the lattice parameter trends were performed using the software TOPAS v6.[12] Lattice parameters for LiTFSI·H_2O were determined by Rietveld refinement using a simple axial model plus Gaussian and Lorentzian crystallite size and strain broadening parameters to fit the profile. The background was described using Chebychev polynomials of 6^{th} order with an additional broad Gaussian peak added to fit the more prominent liquid diffuse scattering present in higher temperature datasets. Finally, a spherical harmonics correction of second order was added to improve the fit to relative intensities, also likely due to some preferred orientation problems. The lattice parameters were fit for LiTFSI using a Pawley refinement, because the relative intensity errors due to poor orientation statistics made Rietveld refinement (and quantification) impossible. In this case, only Gaussian size and strain broadening were used.

Additional measurements at room temperature were performed using a transmission stage, in which the sample powder was sealed with wax between two plastic windows and measured with the sample spinning around an axis parallel to the beam. This geometry gave better orientation statistics, giving improved relative peak intensities. However, this geometry did not allow for temperature control, and the sample could not be completely sealed against air, becoming amorphous within a short period, presumably after taking up water from the air.

2. Figures and Tables

Molality	**21 m**	**30 m**	**40 m**	**55.5 m**
Solidifying Point（℃）	9.6	36.2	26.8	31.3

Melting Points （℃）	6.6	10 & 46.4	51.4	46.2

Table S1. The melting and solidifying points of LiTFSI-H_2O system with different salt concentrations, measured by DSC.

Structure	α_{X1} **(MK^{-1})**	α_{X2} **(MK^{-1})**	α_{X3} **(MK^{-1})**	α_{V} **(MK^{-1})**
LiTFSI·H_2O	44(2)	73(6)	90(4)	214(12)
LiTFSI	-5(3)	41(2)	149(4)	187(4)

Table S2: The principle coefficients of thermal expansion (linear and volumetric) as determined using the PASCAL software. The directions of the components are provided in the SI.

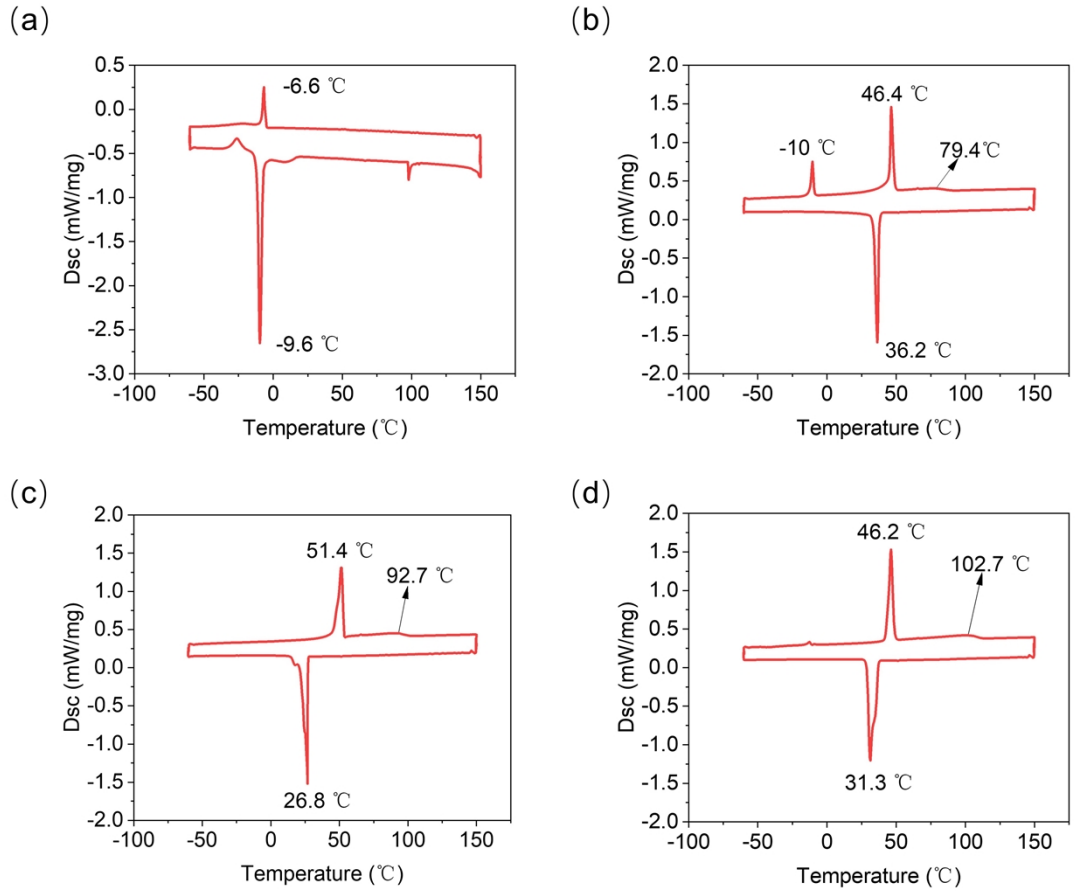

Figure S1. DSC measurement of LiTFSI-H2O system with different salt concentration, (a) 21 m, (b) 30 m, (c) 40 m, (d) 55.5 m.

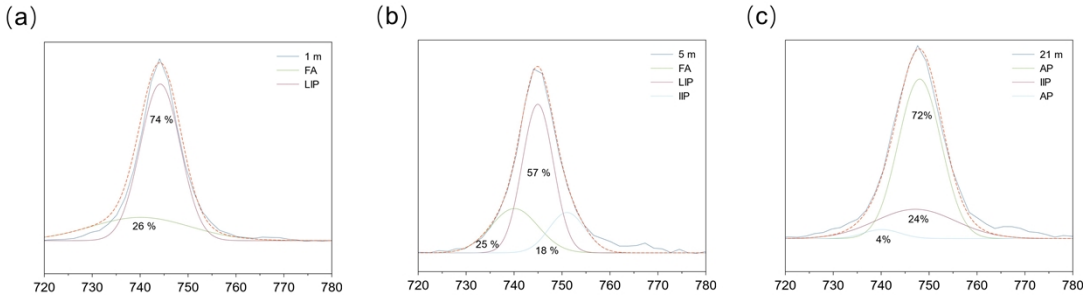

Figure S2. Raman spectra of (a) 1 m (b) 5 m and (c) 21 m LiTFSI WIS sample.

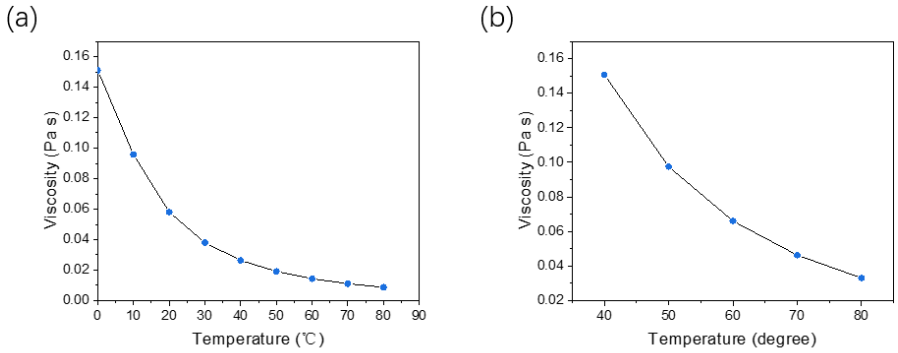

Figure S3. The viscosity of (a) 21 m and (b) 30 m LiTFSI-H_20 at different temperatures.

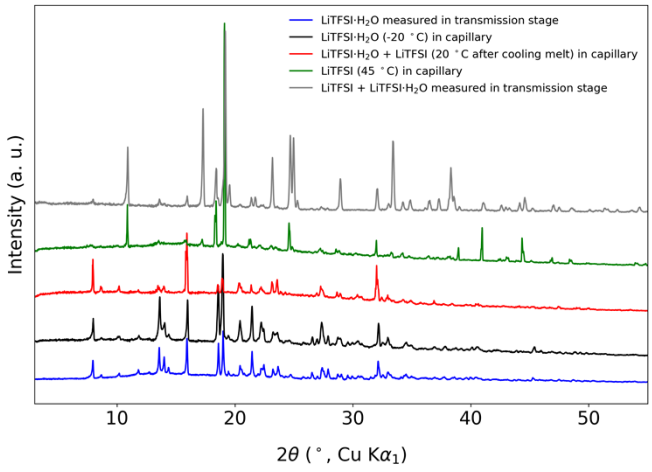

Figure S4. The comparison of the XRD patterns at various temperatures. Issues with poor orientational sampling statistics can be seen by the relative intensities and even absence of some peaks for the LiTFSI pattern measured in capillary (green) versus in the transmission stage (grey).

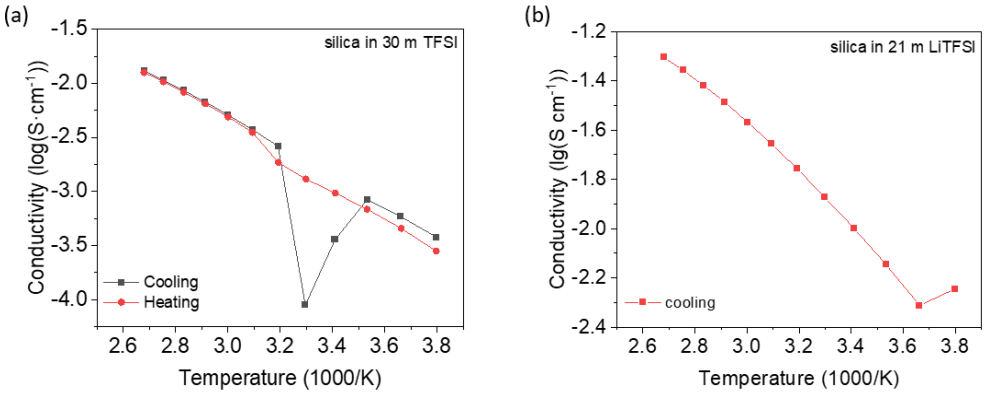

Figure S5 . The conductivity of (a) 30 m and (b) 21 m LiTFSI solution with SiO_2 nanoparticle (silica) additive.

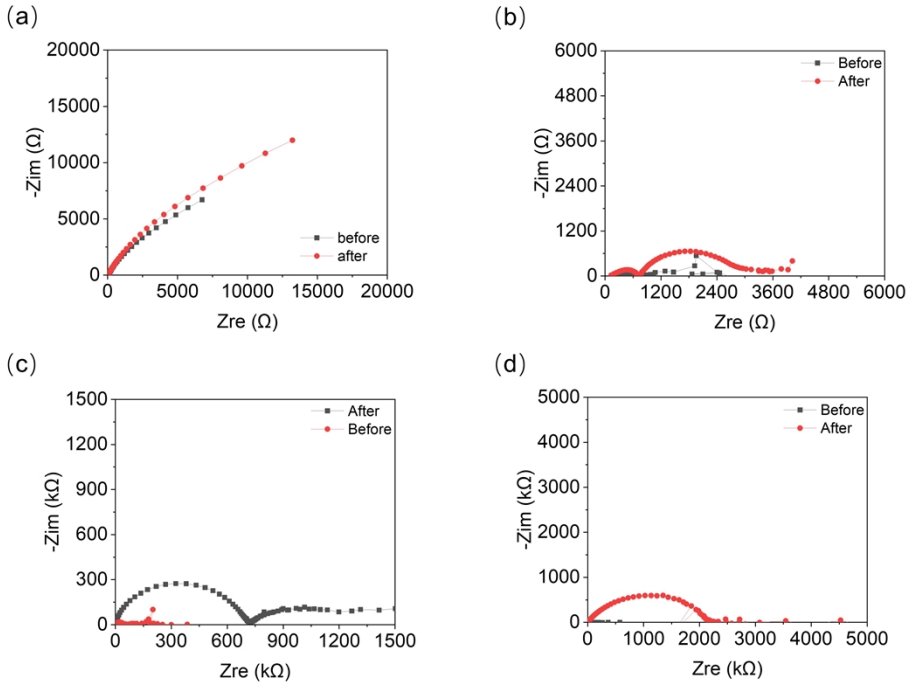

Figure S6. Full-scale EIS Nyquist plot of (a) 21 m (b) 30 m (c) 40 m (d) 55.5 m LiTFSI-H_2O.

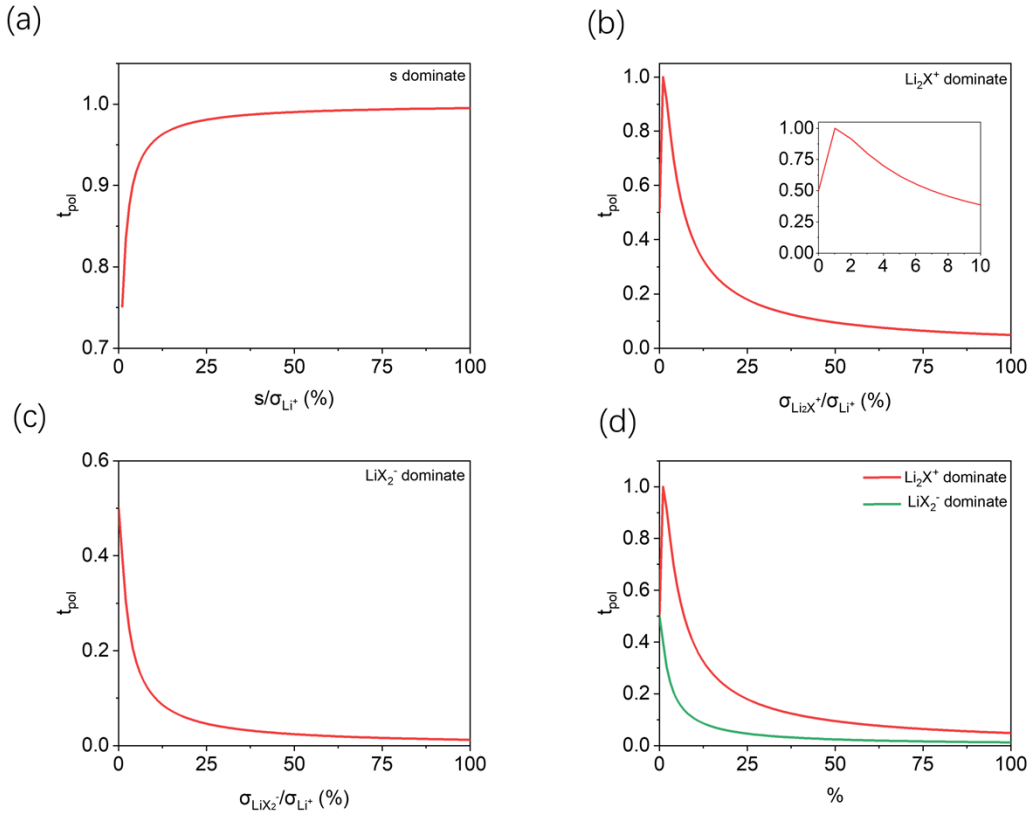

Figure S7. The relationship between contribution of each component and the polarization transference number based on theoretical calculation in supplementary information, (a) s dominate; (b)Li_2X^+ dominate; (c)LiX_2^- dominate;(d) the comparison between b and c.

Figure S8. Photos of water-in-salt electrolytes: (left) 21 m, (right) 40 m.

Thermal Expansion Output from PASCAL software.

Output for LiTFSI·H_2O (-20-35 °C)

			Direction		
Axes	**α(MK^{-1})**	**σα (MK^{-1})**	**a**	**b**	**c**
X_1	44.4148	1.8542	0.1307	0.7064	-0.6957
X_2	73.1010	5.5325	-0.6137	0.2511	0.7485
X_3	89.8411	4.1130	0.7193	0.1932	0.6673
V	213.5664	11.6817			

% change in length

T	X_1	X_2	X_3	$X_{1,calc}$	$X_{2,calc}$	$X_{3,calc}$
253.1500	0.0000	0.0000	0.0000	-0.0084	-0.0216	-0.0044
258.1500	0.0215	0.0344	0.0500	0.0138	0.0150	0.0405
263.1500	0.0581	0.0843	0.1290	0.0360	0.0515	0.0854
268.1500	0.0336	0.0524	0.0866	0.0582	0.0881	0.1303
273.1500	0.0732	0.1163	0.1674	0.0804	0.1246	0.1752
278.1500	0.0885	0.1452	0.2141	0.1027	0.1612	0.2202
283.1500	0.1183	0.1782	0.2617	0.1249	0.1977	0.2651
288.1500	0.1475	0.2053	0.3055	0.1471	0.2343	0.3100
293.1500	0.1632	0.2566	0.3424	0.1693	0.2708	0.3549
298.1500	0.1972	0.2870	0.3946	0.1915	0.3074	0.3998
303.1500	0.2177	0.3552	0.4323	0.2137	0.3439	0.4448
308.1500	0.2464	0.4387	0.5279	0.2359	0.3805	0.4897

Volume

T	V (Å^3)	V_{lin} (Å^3)
253.1500	1921.0816	1920.1190
258.1500	1923.1167	1922.1704
263.1500	1926.2987	1924.2218
268.1500	1924.3966	1926.2732
273.1500	1927.9452	1928.3246
278.1500	1929.6973	1930.3760
283.1500	1931.8261	1932.4274
288.1500	1933.7535	1934.4788
293.1500	1935.7589	1936.5302
298.1500	1938.0130	1938.5816
303.1500	1940.4554	1940.6330
308.1500	1944.4774	1942.6844

Input

T	σT	a	b	c	α	β	γ

308.15	2	11.5121	17.7763	9.7848	90.0207	99.5668	99.8664
303.15	2	11.5053	17.7678	9.776	90.0441	99.5654	99.8962
298.15	2	11.4991	17.7614	9.7721	90.0561	99.5265	99.9193
293.15	2	11.4947	17.757	9.7676	90.0441	99.535	99.9363
288.15	2	11.4893	17.7518	9.7646	90.0662	99.5237	99.9327
283.15	2	11.4856	17.7481	9.7606	90.0595	99.5278	99.948
278.15	2	11.4819	17.7427	9.7564	90.0655	99.5342	99.9553
273.15	2	11.4779	17.7391	9.7533	90.0745	99.5456	99.9552
263.15	2	11.4734	17.7354	9.7508	90.0826	99.5503	99.9484
268.15	2	11.4692	17.7321	9.7468	90.0862	99.5524	99.9538
258.15	2	11.4648	17.7283	9.7463	90.0967	99.5607	99.949
253.15	2	11.4608	17.7238	9.7424	90.0991	99.568	99.9592

Output for LiTFSI·H_2O (-20-35 °C)

			Direction		
Axes	**α(MK^{-1})**	**σα (MK^{-1})**	**a**	**b**	**c**
X_1	-5.0680	2.9872	-0.0000	1.0000	-0.0000
X_2	41.2701	1.5226	-1.0000	0.0000	0.0000
X_3	148.7544	3.6396	-0.0000	-0.0000	1.0000
V	186.5780	4.0360			

% change in length

T	X_1	X_2	X_3	$X_{1,calc}$	$X_{2,calc}$	$X_{3,calc}$
253.1500	0.0000	0.0000	0.0000	-0.0211	-0.0083	-0.0082
258.1500	-0.0110	0.0186	0.0636	-0.0236	0.0124	0.0662
263.1500	-0.0110	0.0557	0.1870	-0.0262	0.0330	0.1405
268.1500	-0.0165	0.0361	0.1346	-0.0287	0.0536	0.2149
273.1500	-0.0312	0.0733	0.2778	-0.0312	0.0743	0.2893
278.1500	-0.0881	0.0857	0.3981	-0.0338	0.0949	0.3637
283.1500	-0.0826	0.1105	0.4722	-0.0363	0.1155	0.4381
288.1500	-0.0679	0.1342	0.5216	-0.0388	0.1362	0.5124
293.1500	-0.0533	0.1549	0.5765	-0.0414	0.1568	0.5868
298.1500	-0.0275	0.1776	0.6265	-0.0439	0.1774	0.6612
303.1500	-0.0073	0.1972	0.6895	-0.0464	0.1981	0.7356
308.1500	0.0606	0.2158	0.7567	-0.0490	0.2187	0.8099
313.1500	-0.0992	0.2220	0.9703	-0.0515	0.2393	0.8843
318.1500	-0.1010	0.2498	1.0042	-0.0540	0.2600	0.9587
323.1500	-0.0808	0.2777	1.0524	-0.0566	0.2806	1.0331
328.1500	-0.0551	0.3056	1.0944	-0.0591	0.3012	1.1075
333.1500	-0.0312	0.3510	1.1505	-0.0616	0.3219	1.1818

Volume

T	V (Å^3)	V_{lin} (Å^3)
253.1500	854.5763	854.2075
258.1500	855.1843	855.0047
263.1500	856.5575	855.8019
268.1500	855.8939	856.5991
273.1500	857.3104	857.3964
278.1500	857.9568	858.1936
283.1500	858.8497	858.9908
288.1500	859.6019	859.7880
293.1500	860.3755	860.5853
298.1500	861.2199	861.3825
303.1500	862.1016	862.1797
308.1500	863.4239	862.9769
313.1500	863.9259	863.7742
318.1500	864.4409	864.5714
323.1500	865.2683	865.3686
328.1500	866.0911	866.1658
333.1500	867.1718	866.9631

Input

T	σT	a	b	c	α	β	γ
333.15	2	9.7203	5.4439	16.3876	90	90	90
328.15	2	9.7159	5.4426	16.3785	90	90	90
323.15	2	9.7132	5.4412	16.3717	90	90	90
318.15	2	9.7105	5.4401	16.3639	90	90	90
313.15	2	9.7078	5.4402	16.3584	90	90	90
308.15	2	9.7072	5.4489	16.3238	90	90	90
303.15	2	9.7054	5.4452	16.3129	90	90	90
298.15	2	9.7035	5.4441	16.3027	90	90	90
293.15	2	9.7013	5.4427	16.2946	90	90	90
288.15	2	9.6993	5.4419	16.2857	90	90	90
283.15	2	9.697	5.4411	16.2777	90	90	90
278.15	2	9.6946	5.4408	16.2657	90	90	90
273.15	2	9.6934	5.4439	16.2462	90	90	90
263.15	2	9.6917	5.445	16.2315	90	90	90
268.15	2	9.6898	5.4447	16.223	90	90	90
258.15	2	9.6881	5.445	16.2115	90	90	90
253.14999999999998	2	9.6863	5.4456	16.2012	90	90	90

References

1. Popovic, J., Pfaffenhuber, C., Melchior, J. & Maier, J. Determination of individual

contributions to the ionic conduction in liquid electrolytes: Case study of LiTf/PEGDME-150. *Electrochem. Commun.* **60**, 195–198 (2015).

2. Popovic, J. *et al.* High Lithium Transference Number Electrolytes Containing Tetratriflylpropene's Lithium Salt. *J. Phys. Chem. Lett.* **9**, 5116–5120 (2018).
3. Maier, J. Salt concentration polarization of liquid electrolytes and determination of transport properties of cations, anions, ion pairs and ion triples. *Electrochimica Acta* **129**, 21–27 (2014).
4. Harris, R. K. *et al.* Further conventions for NMR shielding and chemical shifts (IUPAC Recommendations 2008). *Pure Appl. Chem.* **80**, 59–84 (2008).
5. Bielecki, A. & Burum, D. P. Temperature dependence of207Pb MAS spectra of solid lead nitrate. an accurate, sensitive thermometer for variable-temperature MAS. *J. Magn. Reson. A* **116**, 215–220 (1995).
6. Massiot, D. *et al.* Modelling one-and two-dimensional solid-state NMR spectra. *Magn. Reson. Chem.* **40**, 70–76 (2002).
7. Rohonczy, J. Bruker BioSpin GmbH: Rheinstetten. (2009).
8. Tanner, J. E. Use of the stimulated echo in NMR diffusion studies. *J. Chem. Phys.* **52**, 2523–2526 (1970).
9. Stejskal, E. O. & Tanner, J. E. Spin diffusion measurements: spin echoes in the presence of a time-dependent field gradient. *J. Chem. Phys.* **42**, 288–292 (1965).
10. Aihara, Y. *et al.* Ion transport properties of six lithium salts dissolved in γ-butyrolactone studied by self-diffusion and ionic conductivity measurements. *J. Electrochem. Soc.* **151**, A119 (2003).

11. Price, W. S. & Kuchel, P. W. Effect of nonrectangular field gradient pulses in the Stejskal and Tanner (diffusion) pulse sequence. *J. Magn. Reson.* **94**, 133–139 (1991).

12. Coelho, A. A. TOPAS and TOPAS-Academic: an optimization program integrating computer algebra and crystallographic objects written in C++. *J. Appl. Crystallogr.* **51**, 210–218 (2018).